DOI: 10.1109/TMECH.2022.3156168

Autonomous Locomotion Trajectory Shaping and Nonlinear Control for Lower-Limb Exoskeletons

Mojtaba Sharifi, *Member, IEEE,* Javad K. Mehr, *Student Member, IEEE,* Vivian K. Mushahwar, *Member, IEEE,* Mahdi Tavakoli, *Senior Member, IEEE*

***Abstract*—This paper presents a strategy for autonomous locomotion trajectory planning for high-level control of lower-limb exoskeletons by defining a novel set of adaptive central pattern generators (ACPGs) to facilitate safe and compliant interaction with the human. A time-varying bounded-gain adaptive (TBA) disturbance observer is designed for estimating the human-robot interaction (HRI) needed for online CPG-based trajectory shaping and low-level nonlinear trajectory tracking control. The proposed ACPG dynamics for each exoskeleton joint updates the motion frequency and amplitude based on the observed HRI torque, which is also coupled with adjacent joints' CPGs to regulate their phase differences in real-time. An integrated Lyapunov analysis is conducted to ensure the closed-loop system's stability and uniformly ultimately boundedness (UUB) of both the tracking error and the torque estimation error in the controlled exoskeleton. Experimental studies are performed with an able-bodied human wearer by applying arbitrary torques on the exoskeleton's joints in order to evaluate the proposed autonomous control strategy in online adjustment and personalization of the locomotion.**

***Index Terms*—Adaptable central pattern generators (ACPGs), gait trajectory planning, time-varying bounded-gain adaptive (TBA) disturbance observer, human-robot interaction (HRI), autonomous nonlinear control**

I. Introduction

MILLIONS of people all over the world are currently experiencing neurological impairments, including stroke, spinal cord injury, multiple sclerosis, and cerebral palsy [1]. Assisting these individuals in daily living activities by robotic systems (e.g., exoskeletons) will enhance their quality of life, and facilitate rehabilitation. In comparison with traditional physical therapies, powered exoskeletons have the ability to provide frequent, consistent and long-term assistance with minimal engagement of a therapist [2]. This leads to a lower cost and higher efficiency of task execution by accurately rendering the required assistance level to any subject with specific neurological conditions. Moreover, precise measurements of human limb movements can be collected for continuous monitoring of the user's condition by deploying embedded sensors in the exoskeleton's structure.

Due to the inability of passive orthoses to assist people with movement disorders to realize an appropriate upright walking, powered lower-limb exoskeletons (such as Indego [3], ReWalk [4], and GEMS [5]) have been designed and fabricated as an alternative solution [6]. Although these developed exoskeletons are now deployed in some clinical settings to assist and rehabilitate people [6], a compliant interaction between the robot and wearer is an issue that still needs to be resolved [7]. To address this challenge, industrial exoskeletons such as Honda SML [8], Samsung Electronics [9], and Keeogo [10] have benefited from adaptive strategies to shape the exoskeleton's walking trajectories based on user-specific gait patterns. However, these exoskeletons have not utilized any online estimation of HRI in locomotion planning and they were designed for assisting/rehabilitating only one single joint (hip or knee). Control strategies for lower-limb exoskeletons play the most critical role in providing safe and comfortable interaction between the wearer and the robot, which are divided into high-level and low-level categories. The motion trajectory and sequence of locomotion are planned at the high level (based on the user's intention and motor capacity) and are implemented at the low level using position, force or impedance controllers. To date, some studies have developed control schemes in both levels, while others focused only on the low-level control design by employing pre-specified reference gait trajectories [11], [12], [13].

Different nonlinear methods were proposed in the literature for high-level motion planning of robotic systems, including dynamic movement primitives (DMPs) and central pattern generators (CPGs). DMPs were defined in [14] as a combination of several differential equations to mimic the stream of movements captured from humans and animals. Researchers employed DMPs for locomotion trajectory generation and position/torque control of powered lower-limb exoskeletons [15], [16], [17]. Yuan et al. [15] have recruited a point-attractor DMP structure for the trajectory shaping of hip and knee joints, augmented by reinforcement learning (RL) to update the DMP parameters with the purpose of minimizing the error between the target and actual trajectories [15]. With a similar objective, the locally weighted regression (LWR) method was

Manuscript received May 31, 2021. Manuscript received May 31, 2021; Revised: October 21, 2021; Accepted: November 28, 2021.*(Corresponding author: Mojtaba Sharifi)*

Mojtaba Sharifi and Javad K. Mehr are with the Department of Electrical and Computer Engineering, and the Department of Medicine, University of Alberta, Edmonton, Alberta, Canada (e-mail: M.Sharifi@ualberta.ca; J.Khodaeimehr@ualberta.ca)

Mojtaba Sharifi is with the Department of Mechanical Engineering, San Jose State University, San Jose, California 95192-0087 (e-mail: Mojtaba.Sharifi@sjsu.edu)

Vivian K. Mushahwar is with the Department of Medicine, Division of Physical Medicine and Rehabilitation, University of Alberta, Edmonton, Alberta, Canada T6G 2E1 (e-mail: Vivian.Mushahwar@ualberta.ca)

Mahdi Tavakoli is with the Department of Electrical and Computer Engineering, University of Alberta, Edmonton, Alberta, Canada T6G 1H9 (e-mail: Mahdi.Tavakoli@ualberta.ca)

All authors are with the Sensory Motor Adaptive Rehabilitation Technology (SMART) Network, University of Alberta, Edmonton, Alberta, Canada T6G 2E1

suggested in [16] to regulate the weights of basis functions in the DMP dynamics. Huang et al. [17] developed another DMP structure by embedding the HRI torque in the point-attractor DMP dynamics to shape the pilot locomotion trajectory online.

CPGs are defined as connected networks that can produce coordinated patterns of a rhythmic activity based on non-oscillatory inputs [18], [19]. This dynamical system, inspired by salamanders' rhythmic motions, was suggested for robotic systems by Ijspeert [20] in 2007. The inherent feature of CPGs in generating oscillatory movements benefited the high-level control of exoskeletons in several research studies [21]. Fang et al. [22] used this mathematical tool to produce the desired trajectories for the hip and knee joints of a 4-DOF exoskeleton, where the CPG dynamic parameters were adjusted using a genetic algorithm (GA) offline. Similar GA-based CPGs were devised in [23] to generate rhythmic patterns for torque control of the hip and knee joints in order to have steady-state walking for a lower-limb exoskeleton. The knee stiffness was regulated in terms of the normal ground reaction force by exciting two stiffening CPG units [23]. Another offline trajectory regulation was defined in [24] using Matsuoka-style CPGs in which the HRI force was estimated by inverse dynamics analysis, and two fuzzy-logic regulators identified appropriate exoskeleton's impedance (stiffness and damping). Gui et al. [25] utilized able-bodied motion data to generate pre-specified trajectories of the knee and hip joints taking advantage of CPGs and admittance control to facilitate pre-specified flexibility in terms of the measured electromyography (EMG) signals. A combination of functional electrical stimulation (FES) and torque control of a lower-limb exoskeleton was suggested in [26] to develop a hybrid rehabilitation system for the knee joint. Two CPGs were used to generate fixed oscillatory knee movements, which were then fed to the FES feedforward controller and exoskeleton feedback controller to realize a rhythmic knee motion [26].

According to differences between users in their functional capacity and behavior, variations of their intention during the task in each situation, and effects of environmental factors (surface slope and condition), the online investigation of physical human force/torque is highly demanded in realizing safe and comfortable HRI [27], [28]. Thereby, determining the interaction force/torque between the human and exoskeleton is a crucial requirement and, at the same time, a technical challenge for designing high-level motion planning and low-level torque control. Estimating HRI torque using EMG signals acquired from human muscles is an approach commonly employed for this purpose [11], [25], [29]. Although human torque can be estimated from EMG signals, the obtained results suffer from considerable inaccuracy due to calibration, muscle fatigue, electrode positioning and muscle-skin conductivity variation [16]. To overcome these issues, force/torque sensors were utilized as an alternative solution in some research work [30], [26], [31], [32]. Despite the accurate data of these sensors, their cost and difficulty in embedding them between the human body and exoskeleton drove researchers and manufacturers to rely more on estimation methods instead of direct measurement of the interaction force/torque. Dynamic modeling of musculoskeletal systems was also utilized to estimate the passive portion of the interaction torque [17], [16], [24], [33]; however, its active part is either neglected or estimated from force/torque measurements. To address these measurement challenges autonomously, disturbance observers were developed for online estimation of HRI torque [34], [35], [36]. Pan et al. [34] designed a nonlinear model-based observer to compensate for the external torque in their low-level controller for trajectory tracking. In another study [35], a nonlinear disturbance observer was investigated to estimate the human torque, which was used in the proportional–derivative (PD) torque control law of a knee-joint exoskeleton with series elastic actuators (SEAs). A similar torque observer was developed in [36] for the implementation of a sliding-mode controller (SMC) in the low-level to track the response of an admittance model.

In the present study, a novel nonlinear autonomous control strategy is proposed to realize compliant, safe and case-specific physical human-robot interaction (pHRI) for lower-limb exoskeletons by integrating ACPGs and a time-varying bounded-gain adaptive (TBA) disturbance observer. At the high level of this strategy, new ACPGs are investigated to shape rhythmic locomotion trajectories in real-time based on the interaction between the human (wearer) and exoskeleton. The initial gait trajectory is extracted from typical gait data of able-bodied individuals and mathematically represented by an eight-term expansion of the Fourier series. For the first time, the nonlinear ACPGs' dynamics is augmented by HRI torque estimation in order to update the amplitude, frequency, and phase of walking based on the wearer's intention (physical behavior). To this end, a new multi-layer TBA disturbance observer is formulated to estimate HRI torque to be employed in (a) the low-level torque controller for motion tracking, and (b) the high-level CPG-based locomotion planning for rendering human flexibility. The stability of this autonomous pHRI system, and the uniform ultimate boundedess (UUB) of trajectory tracking error and torque estimation error are guaranteed through a comprehensive Lyapunov analysis. The main contributions of this strategy over previous ones can be summarized as:

- The HRI torque is employed in the defined nonlinear CPG dynamics to generate adaptable reference trajectories for the gait cycles. Previous CPG-based controllers [22], [23], [24], [25], [26] for lower-limb exoskeletons have not taken HRI torque into account in their CPG structures. This feature of the proposed strategy makes the exoskeleton significantly compliant with the wearer's physical interaction and enhances safety by raising her/his high-level authority in motion planning.
- The nonlinear multi-layer TBA disturbance observer is designed to facilitate exoskeletons' stability regarding the UUB of both tracking and estimation errors. Previous disturbance observer designs have not taken into account the stability of the controlled system [34]. Other disturbance observers [35], [36] have been developed for a single-joint (knee) exoskeleton with a scalar dynamic model and fixed adaptation gains that need to be determined through trial-and-error. In this study, a TBA disturbance observer

is developed for multi-DOF exoskeletons with a nonlinear coupled matrix formulation. Moreover, a nonlinear adaptation is defined for automated online regulation of the time-varying bounded gain in the observer's structure to facilitate smooth torque estimation. In comparison with previous observers [35], [36], a first-order dynamics is also employed in this scheme for intermediate variables of the combined exoskeleton-human limb system to diminish undesired noise in these signals and avoid reflecting it in the torque observation.

The rest of this paper is organized as follows. The nonlinear dynamic model of the lower limb exoskeleton and the structure of the ACPGs (high-level control) are presented in Sec. II. The proposed TBA disturbance observer, the low-level torque control strategy and the closed-loop system's stability are explained in Sec. III. The experimental evaluations of the developed autonomous control scheme are presented in Sec. IV and discussed in Sec. V. The concluding remarks are provided in Sec. VI.

II. Exoskeleton Dynamics and Adaptive CPG-Based Online Trajectory Shaping

The nonlinear dynamics of a lower-limb exoskeleton shown in Fig. 1 with n joints together with the human user is given as

$$M_q(q)\ddot{q} + C_q(q)\dot{q} + G_q(q) = \tau_{mot} + \tau_{hum} \tag{1}$$

where q is the vector of exoskeleton joints' position, $M_q(q)$ is the inertia matrix, $C_q(q)$ is the matrix of Coriolis, centrifugal and damping terms, $G_q(q)$ is the vector of gravitational torques, τ_{con} is the exoskeleton's motor torque, and τ_{hum} is the human torque generated by his/her muscles' contractions.

Property 1: The inertia matrix M_q is positive definite and uniformly bounded such that there are a min-bound on the minimum singular value and a max-bound on the maximum singular value of this matrix [37]:

$$0 < M_1 \leq \|M_q\| \leq M_2 < \infty \tag{2}$$

where M_1 and M_2 are the uniform bounds, and $\|.\|$ is the induced norm. The matrix $\dot{M}_q - 2C_q$ is skew symmetric, and the left side of (1) can be linearly parameterized [38], [39] as

$$M_q(q)\phi_1 + C_q(q)\phi_2 + G_q(q) = Y_q(\phi_1, \phi_2, q, \dot{q})\theta_q \tag{3}$$

in which Y_q is the regressor matrix defined in terms of known variables including ϕ_1 and ϕ_2, and θ_q is the vector of unknown parameters of the robot dynamics.

For the high-level control of the exoskeleton, a learning-based locomotion path generation is developed by defining an ACPG, as illustrated schematically in Fig. 2. To this end, human physical behavior is taken into account during the motion and interaction with the exoskeleton. In order to interpret this behavior, the estimated HRI energy is defined for each joint i as follows:

$$P_i(t) = \int_0^t \tau_{HRI_i}(t)\ \dot{q}_i(t)\ dt \tag{4}$$

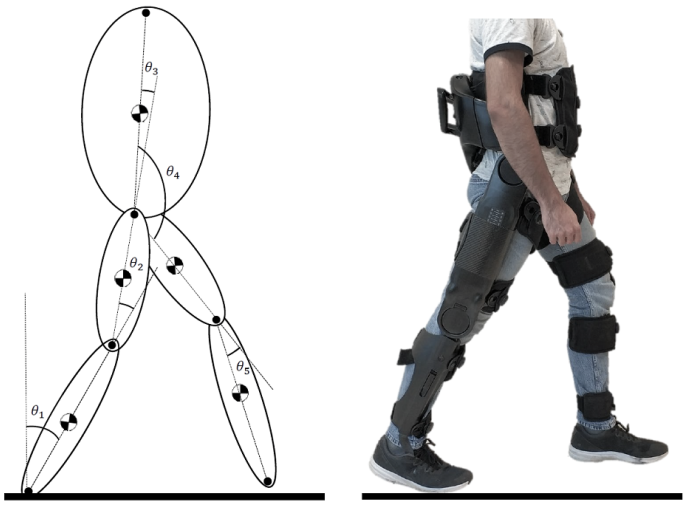

Fig. 1. The employed lower-limb exoskeleton (Indego by Parker Hannifin Corporation), and joint consequences from the stance leg to the swing one based on pinned (point-feet) model

where $\dot{q}_i(t)$ is the velocity of the joint $i = 1, ..., n$, and $\tau_{HRI_i}(t)$ is the estimated value of the human torque on this joint of the exoskeleton after applying a dead-zone function:

$$\tau_{HRI_i} = \begin{cases} \hat{\tau}_{hum_i} - \tau_{thr_{pos}} & for \quad \hat{\tau}_{hum_i} > \tau_{thr_{pos}} \\ 0 & for \quad \tau_{thr_{neg}} \leq \hat{\tau}_{hum_i} \leq \tau_{thr_{pos}} \\ \hat{\tau}_{hum_i} - \tau_{thr_{neg}} & for \quad \hat{\tau}_{hum_i} < \tau_{thr_{neg}} \end{cases} \tag{5}$$

in which $\tau_{thr_{pos}}$ and $\tau_{thr_{neg}}$ are the positive and negative thresholds of this dead-zone for the estimated human torque $\hat{\tau}_{hum_i}$. In other words, if human users apply any torque larger than these thresholds, they will be able to modify the locomotion trajectory's characteristics as explained below.

Suppose that both τ_{HRI_i} and $\dot{q}_i$ in (4) are either positive or negative. In this case, the operator applies a torque/force in the same direction as the joint's motion by injecting energy into the system ($\dot{P}_i(t) > 0$) to accelerate this movement. On the other hand, $\dot{P}_i(t) < 0$ implies dissipating energy by opposing torque/force of the human user with respect to the motion. Accordingly, the proposed ACPG dynamics for the phase $\theta_i(t)$, frequency $\omega(t)$ and amplitude $\mu(t)$ of locomotion trajectories is formulated as a coupled system of nonlinear oscillators as

$$\begin{aligned} \dot{\theta}_i(t) =& \omega(t) + \sum_{j=1}^{m_i} \gamma_{ij}(\dot{P}_i - \dot{P}_j) \\ &+ \sum_{j=1}^{m_i} v_{ij}\ sin(\theta_i(t) - \theta_j(t) - \phi_{ij}) \\ \ddot{\omega}(t) =& \beta_\omega(\frac{\beta_\omega}{4}(\Omega + \sum_{k=1}^{n} \psi_k P_k - \omega(t)) - \dot{\omega}(t)) \\ \ddot{\mu}(t) =& \beta_\mu(\frac{\beta_\mu}{4}(A + \sum_{k=1}^{n} \lambda_k P_k - \mu(t)) - \dot{\mu}(t)) \end{aligned} \tag{6}$$

in which m_i is the number of adjacent joints to the joint i, and n is the number of all joints. γ_{ij}, ψ_k and λ_k are constant factors of HRI energy effect on phase, frequency and amplitude variations of locomotion, respectively. v_{ij}, β_ω and

β_μ are other constant parameters of this dynamics. The desired trajectory for the joint i of the exoskeleton is defined as

$$q_{d_i}(t) = \mu(t)(a_{i_0} + \sum_{l=1}^{N_i}(a_{i_l}\cos(l\theta_i(t)) + b_{i_l}\sin(l\theta_i(t))) \quad (7)$$

where a_{i_l} and b_{i_l} are the coefficients of Fourier series (with N_i terms) to initially match the desired trajectory of the joint i to a typical walking trajectory, as demonstrated in Fig. 2. The amplitude and phase of these oscillatory motions are updated in real-time by $\mu(t)$ and $\theta_i(t)$ obtained from (7). Note that the generated reference trajectory in (7) is continuous in time and differentiable, which are beneficial features for the control scheme presented in the next section. To perceive the proposed adaptive autonomous trajectory shaping (6) and (7), the following characteristics can be mentioned.

A coupling between all joints is facilitated, having the same principal frequency of $\omega(t)$ to synchronize generated locomotion trajectories. The scaling factor of these trajectories is specified to be the same $\mu(t)$, while the initial coefficients of the Fourier series a_{i_l} and b_{i_l} for each joint i are determined from typical experimental data. This mutual adjustment of $\omega(t)$ and $\mu(t)$ for all joints guarantees synchronized multi-DOF locomotion and provides the appropriate overground motion of the feet in the Cartesian space.

The HRI energy $P_k(t)$ injected to or dissipated from the system by the wearer through each joint k of the exoskeleton can affect the frequency $\omega(t)$ and the amplitude coefficient $\mu(t)$ of locomotion trajectory. Based on this feature, human users can physically demonstrate their compliance or resistance by applying accelerating or decelerating torques with respect to the implemented gait trajectories of all n joints of the exoskeleton. This effect can be regulated by ψ_k and λ_k as the authority factors of each joint torque over the generation of the overall gait pattern.

The other adjustable coupling in the proposed CPG-based trajectory shaping is the online variation of phase lead/lag between adjacent joints. The difference between the rate of exerted energy by the human user on two adjacent joints $(\dot{P}_i - \dot{P}_j)$ will affect the phase difference between these joints (i and j). In this regard, the human behavior on accelerating/decelerating the motion of one joint i with respect to its adjacent joints is perceived by the HRI energy estimation P_i. Another harmonic term for connecting ACPGs correspond to adjacent joints is facilitated by $sin(\theta_i(t) - \theta_j(t) - \phi_{ij})$ based on the scheme presented in [40]. The coefficients γ_{ij} and v_{ij} specify the gains of this synchronized phase variation for each joint.

Regarding the requirement of torque estimation $\hat{\tau}_{hum_i}$ in the proposed ACPG formulations (4), (5) and (6), a new adaptive disturbance observer is defined in the next section together with a nonlinear low-level controller for trajectory tracking.

III. TBA Disturbance-Observer-Based Control

In this section, an autonomous observer-based strategy is developed for the low-level controller of the exoskeleton. In this strategy, the human interaction torque is estimated via a multi-layer TBA disturbance observer in order to be employed in the high-level gait generation (4) and (6). At the same time, this HRI torque estimation is also utilized in the low-level control law for tracking the generated locomotion trajectory, as seen in Fig. 2.

A. Controller and Observer Design

For the purpose of controlling motor torque and estimating HRI torque, the tracking error e_q, its dynamics ϵ_q and the corresponding auxiliary variable $\dot{q}_r$ are defined:

$$\begin{aligned} e_q(t) &= q(t) - q_d(t) \\ \epsilon_q(t) &= \dot{e}_q(t) + \kappa_1 e_q(t) \\ \dot{q}_r(t) &= \dot{q}_d(t) - \kappa_1 e_q(t) \end{aligned} \quad (8)$$

The proposed nonlinear trajectory tracking control law for the exoskeleton's motor torque is formulated as

$$\tau_{mot} = M_q(\ddot{q}_r - \kappa_2\epsilon_q) + C_q\dot{q}_r + G_q - \hat{\tau}_{hum} \quad (9)$$

in which κ_1 and κ_2 are positive constant gains. Substituting the proposed controller (9) in the user-exoskeleton dynamics (1) leads to the following closed-loop dynamics:

$$M_q\dot{\epsilon}_q = -\kappa_2 M_q\epsilon_q - C_q\epsilon_q - \tilde{\tau}_{hum} \quad (10)$$

where $\tilde{\tau}_{hum} = \tau_{hum} - \hat{\tau}_{hum}$ is the HRI torque estimation error. Now, the multi-layer TBA disturbance observer is formulated in a couple of steps for estimation of $\hat{\tau}_{hum}$. The final adaptation law is proposed in (31), and required intermediate variables, their boundedness and mathematical derivations are mentioned as follows. Considering a state variable as $z_1 = \epsilon_q$, the dynamics (10) can be presented as

$$\dot{z}_1 = \Psi(z_1, \hat{\tau}_{hum}) + \chi\,\tau_{hum} \quad (11)$$

in which

$$\Psi = -\kappa_2 z_1 + M_q^{-1}C_q z_1 - M_q^{-1}\hat{\tau}_{hum}\,, \quad \chi = M_q^{-1} \quad (12)$$

Then, the filtered variables z_{1f}, Ψ_f and χ_f are defined, having $\xi > 0$, as

$$\begin{aligned} &\xi\dot{z}_{1f} + z_{1f} = z_1\,, \quad z_{1f}(0) = 0 \\ &\xi\dot{\Psi}_f + \Psi_f = \Psi\,, \quad \Psi_f(0) = 0 \\ &\xi\dot{\chi}_f + \chi_f = \chi\,, \quad \chi_f(0) = 0 \end{aligned} \quad (13)$$

Lemma 1: According to the system dynamics (11) and the filters (13), the manifold $[(z_1 - z_{1f})/\xi - \Psi_f - \chi_f\,\tau_{hum}]$ remains bounded for any finite positive value of ξ and converges to zero if τ_{hum} is constant or $\xi \to 0$.

Proof: Considering (13), the filter $1/(\xi s + 1)$ is applied on (11) as

$$\frac{1}{\xi s+1}[\dot{z}_1] = \frac{1}{\xi s+1}[\Psi] + \frac{1}{\xi s+1}[\chi\,\tau_{hum}] \quad (14)$$

Based on (13) and the swapping lemma [41] for $[1/(\xi s + 1)][\chi\,\tau_{hum}]$, one can rewrite (14) as

$$\frac{z_1 - z_{1f}}{\xi} = \Psi_f + \chi_f\,\tau_{hum} + v_1 \quad (15)$$

where the residual term v_1 is obtained as a filtered version of $\dot{\tau}_{hum}$:

$$v_1 = \frac{\xi}{\xi s+1}[\chi\,\dot{\tau}_{hum}] \quad (16)$$

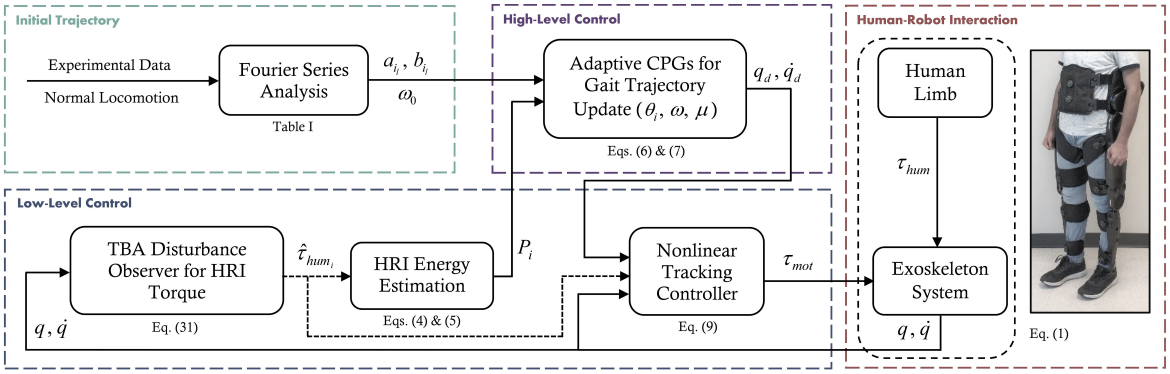

Fig. 2. Autonomous two-level control strategy for lower-limb exoskeletons: Adaptive CPG-based gait trajectory update in high-level and nonlinear torque control in low-level, employing an adaptive HRI torque observer

As a result, when τ_{hum} is constant or $\xi = 0$, it is concluded that $v_1 = 0$. Moreover, since $\chi = M_q^{-1}$ and due to *Property* (2) of the inertia matrix, χ is bounded. Consequently, its filtered version χ_f is also bounded, i.e., $||\chi_f|| \leq \rho_\chi = 1/M_1$. Regarding the boundedness of the human torque $||\tau_{hum}|| \leq \rho_\tau$ and its time derivative $||\dot{\tau}_{hum}|| \leq \rho_{\tau_d}$, v_1 is bounded for any finite value of $\xi > 0$, i.e., $||v_1|| \leq \gamma_1$. ■

The dyanmics of two new intermediate variables [42] are defined for the TBA observer design as

$$\begin{aligned} \dot{F}_1 &= -cF_1 + \chi_f^T \chi_f\,, \quad F_1(0) = 0 \\ \dot{F}_2 &= -cF_2 + \chi_f^T \left(\frac{z_1 - z_{1f}}{\xi} - \Psi_f \right), \quad F_2(0) = 0 \end{aligned} \tag{17}$$

in which c is a positive constant. Two other intermediate variables are also formulated in terms of F_1 and F_2 and the estimated HRI torque $\hat{\tau}_{hum}$ as

$$\begin{aligned} T_1 &= F_1\,\hat{\tau}_{hum} - F_2 \\ T_2 &= \chi_f^T \chi_f\,\hat{\tau}_{hum} - \chi_f^T \left(\frac{z_1 - z_{1f}}{\xi} - \Psi_f \right) \end{aligned} \tag{18}$$

Lemma 2: The defined variables in (18) can be expressed as

$$\begin{aligned} T_1 &= -F_1\,\tilde{\tau}_{hum} + v_2 \\ T_2 &= -\chi_f^T \chi_f\,\tilde{\tau}_{hum} - \chi_f v_1 \end{aligned} \tag{19}$$

where v_1 was defined in (16) and v_2 is presented as

$$v_2 = \int_0^t e^{-c(t-r)} \chi_f^T(r)[\chi_f(r)(\tau_{hum}(t) - \tau_{hum}(r)) + v_1(r)]dr \tag{20}$$

This residual error is bounded as $||v_2|| \leq \gamma_2 = (2\rho_\chi^2 \rho_\tau + \rho_\chi \gamma_1)/c$ in which $||\chi_f|| \leq \rho_\chi$, $||\tau_{hum}|| \leq \rho_\tau$ and $||v_1|| \leq \gamma_1$.

Proof: The time integration of (17) results in

$$\begin{aligned} F_1 &= \int_0^t e^{-c(t-r)} \chi_f^T(r)\chi_f(r)\,dr \\ F_2 &= \int_0^t e^{-c(t-r)} \chi_f^T(r)\chi_f(r) \left(\frac{z_1 - z_{1f}}{\xi} - \Psi_f \right)(r)\,dr \end{aligned} \tag{21}$$

Employing (15) and substituting (21) into (18) leads to Eq. (19) where the boundedness of v_2 is obtained as

$$\begin{aligned} \|v_2\| &\leq \int_0^t e^{-c(t-r)} \left\|\chi_f^T(r)\right\| \left[\|\chi_f(r)\|\,\|\tau_{hum}(t) - \tau_{hum}(r)\| \right. \\ &\quad \left. + \|v_1(r)\|\right] dr \\ &\leq \int_0^t \left(2\rho_\chi^2 \rho_\tau + \rho_\chi \gamma_1\right) e^{-c(t-r)} dr \\ &\leq \frac{2\rho_\chi^2 \rho_\tau + \rho_\chi \gamma_1}{c} = \gamma_2 \end{aligned} \tag{22}$$

■

Lemma 3: The matrix χ_f is persistently exciting (PE) as $\int_0^t \chi_f^T(r)\chi_f(r)\,dr \geq \eta_\chi I$ for $t > 0$ and $\eta_\chi > 0$, and the matrix F_1 in (17) is positive definite, i.e., $\lambda_{min}(F_1) \geq \eta_F > 0$ for $t > 0$.

Proof: Based on the definition of the regressor matrix $\chi = M_q^{-1}$ and *Property* (2) of the inertia matrix M_q, and due to the employed low-pass filter (13) with the stable minimum phase transfer function $1/(\xi s + 1)$ [43], one can write: $||\chi_f||_{min} \geq (1/M_2)$. As a result:

$$\begin{aligned} \int_0^t \chi_f^T(r)\chi_f(r)\,dr &\geq \int_0^t \left\|\chi_f^T\right\|_{min} I\, \|\chi_f\|_{min} I\,dr \\ &\geq \int_0^t \left(\frac{I}{M_2}\right)\left(\frac{I}{M_2}\right) dr = \left(t/{M_2}^2\right) I \end{aligned} \tag{23}$$

Considering $\eta_\chi = t/{M_2}^2$, the first proposition in *Lemma 3* is proven. Now, the variable matrix F_1 in (21) is analyzed as

$$\begin{aligned} F_1 &\geq \int_0^t e^{-c(t-r)} \left\|\chi_f^T\right\|_{min} I\, \|\chi_f\|_{min} I\,dr \\ &\geq \left(\frac{I}{{M_2}^2}\right) \int_0^t e^{-c(t-r)}\,dr = \left(\frac{1 - e^{-ct}}{c{M_2}^2}\right) I \end{aligned} \tag{24}$$

Having $\eta_F = (1 - e^{-ct})/(c{M_2}^2)$, the positive definiteness of F_1 with the minimum singular value of η_F is guaranteed. ■

The nonlinear dynamics of time-varying adaptation gain for the observer is formulated as

$$\dot{\mathscr{H}}_\tau = c\mathscr{H}_\tau - \mathscr{H}_\tau \chi_f^T \chi_f \mathscr{H}_\tau \tag{25}$$

According to the fact that $(d/dt)\mathscr{H}_\tau \mathscr{H}_\tau^{-1} = \dot{\mathscr{H}}_\tau \mathscr{H}_\tau^{-1} + \mathscr{H}_\tau (d/dt)\mathscr{H}_\tau^{-1} = 0$ and using (25), $(d/dt)\mathscr{H}_\tau^{-1} =$

$-c\mathscr{H}_\tau^{-1} + \chi_f^T\chi_f$ and thereby:

$$\begin{aligned}\mathscr{H}_\tau &= \left[e^{-ct}\mathscr{H}_\tau^{-1}(0) + \int_0^t e^{-c(t-r)}\chi_f^T(r)\chi_f(r)\,dr\right]^{-1} \\ &= \left[e^{-ct}\mathscr{H}_\tau^{-1}(0) + F_1\right]^{-1}\end{aligned} \tag{26}$$

Regarding (26), the gain matrix $\mathscr{H}_\tau$ exponentially converges to F_1^{-1}, i.e., $\mathscr{H}_\tau F_1 \to I$.

Lemma 4: The adaptation gain matrix $\mathscr{H}_\tau$ is bounded with lower and upper bounds.

Proof: To investigate the boundedness of the adaptation gain $\mathscr{H}_\tau$, Eq. (26) is rewritten as

$$\mathscr{H}_\tau^{-1}(t) = e^{-ct}\mathscr{H}_\tau^{-1}(0) + F_1(t) \tag{27}$$

Based on *Lemma 3* and positive definiteness of $F_1(t)$,

$$\mathscr{H}_\tau^{-1}(t) \geq \eta_F I \tag{28}$$

On the other hand, due to the upper boundedness of $||\chi_f|| \leq \rho_\chi$, one can conclude from (27) that:

$$\mathscr{H}_\tau^{-1}(t) \leq \mathscr{H}_\tau^{-1}(0) + \rho_\chi^2\int_0^t e^{-c(t-r)}I\,dr \leq \mathscr{H}_0^{-1} + \frac{\rho_\chi^2}{c}I \tag{29}$$

Therefore, the boundedness of time-varying observer gain is perceived from (28) and (29) as

$$R_1 I \leq \mathscr{H}_\tau(t) \leq R_2 I \tag{30}$$

in which $R_1 = 1/(\lambda_{min}(\mathscr{H}_0^{-1}) + \rho_\chi^2/c)$ and $R_2 = 1/\eta_F$ are its upper and lower bounds, respectively. ■

The adaptation (estimation) law for the HRI torque in this nonlinear TBA observer is defined as

$$\dot{\hat{\tau}}_{hum} = -\Gamma_\tau\mathscr{H}_\tau(T_1 + \alpha T_2) \tag{31}$$

where $\Gamma_\tau > 0$ and $\alpha > 0$ are the constant scaling factors.

B. Unified Stability Proof

Theorem: Combining the control law (9) that dictates the motor torque and the observer estimation of the HRI torque (31) for the exoskeleton, the convergence of tracking error ϵ_q and the torque estimation error $\tilde{\tau}_{hum}$ to a compact region is achieved. In other words, the system response is uniformly ultimately bounded (UUB) in tracking the desired locomotion trajectory and estimating the bounded HRI torque.

Proof: The following Lyapunov function candidate is utilized to ensure the stability of controlled exoskeleton:

$$V(t) = \frac{1}{2}\left(\epsilon_q^T M_q\epsilon_q + \Gamma_\tau^{-1}\tilde{\tau}_{hum}^T\mathscr{H}_\tau^{-1}\tilde{\tau}_{hum}\right) \tag{32}$$

and its time derivative is obtained as

$$\begin{aligned}\dot{V}(t) = {}& \epsilon_q^T M_q\dot{\epsilon}_q + \Gamma_\tau^{-1}\tilde{\tau}_{hum}^T\mathscr{H}_\tau^{-1}(\dot{\tau}_{hum} - \dot{\hat{\tau}}_{hum}) \\ &+ \frac{1}{2}\left(\epsilon_q^T\dot{M}_q\epsilon_q + \Gamma_\tau^{-1}\tilde{\tau}_{hum}^T\dot{\mathscr{H}}_\tau^{-1}\tilde{\tau}_{hum}\right)\end{aligned} \tag{33}$$

Substituting the closed-loop dynamics (10), the adaptation gain's time variation (25) and the observer formulas (19) and (31) for the HRI torque into (33) results in

$$\begin{aligned}\dot{V}(t) = {}& -\kappa_2\,\epsilon_q^T M_q\epsilon_q - \epsilon_q^T\tilde{\tau}_{hum} + \frac{1}{2}\,\epsilon_q^T(\dot{M}_q - 2C_q)\epsilon_q \\ &+ \Gamma_\tau^{-1}\tilde{\tau}_{hum}^T\mathscr{H}_\tau^{-1}\big(\dot{\tau}_{hum} \\ &+ \Gamma_\tau\mathscr{H}_\tau(-F_1\,\tilde{\tau}_{hum} + v_2 - \alpha\chi_f^T\chi_f\,\tilde{\tau}_{hum} - \alpha\chi_f v_1)\big) \\ &+ \frac{1}{2}\,\Gamma_\tau^{-1}\tilde{\tau}_{hum}^T(-c\mathscr{H}_\tau^{-1} + \chi_f^T\chi_f)\tilde{\tau}_{hum}\end{aligned} \tag{34}$$

Considering *Property 1* of the exoskeleton dynamics, and the lower and upper bounds of matrices and vectors, one can obtain the following upper bound of $\dot{V}(t)$:

$$\begin{aligned}\dot{V}(t) \leq {}& -\mathscr{D}_\epsilon\,\|\epsilon_q\|^2 - \mathscr{D}_{\tau_1}\,\|\tilde{\tau}_{hum}\|^2 \\ &+ \|\epsilon_q\|\,\|\tilde{\tau}_{hum}\| + \mathscr{D}_{\tau_2}\,\|\tilde{\tau}_{hum}\|\end{aligned} \tag{35}$$

in which the gains $\mathscr{D}_i$ are defined in terms of matrices' and vectors' norms as

$$\begin{aligned}\mathscr{D}_\epsilon &= \kappa_2\,\lambda_{min}(M_q) = \kappa_2 M_1 \\ \mathscr{D}_{\tau_1} &= \eta_F + \frac{\alpha}{M_2^2} + \frac{c}{\Gamma_\tau\,R_2} - \frac{1}{\Gamma_\tau\,M_1^2} \\ \mathscr{D}_{\tau_2} &= \frac{\rho_{\tau_d}}{\Gamma_\tau\,R_1} + \gamma_2 + \frac{\alpha\gamma_1}{M_1^2}\end{aligned} \tag{36}$$

As a result, the time derivative of the Lyapunov function is negative definite $\dot{V}(t) < 0$ outside of this compact region:

$$\begin{aligned}\|\epsilon_q\| &\leq \frac{-\mathscr{B}_2 + \sqrt{\mathscr{B}_2^2 + 4\mathscr{B}_1\mathscr{B}_3}}{2\mathscr{B}_1} \\ \|\tilde{\tau}_{hum}\| &\leq \frac{-\mathscr{B}_5 + \sqrt{\mathscr{B}_5^2 + 4\mathscr{B}_4\mathscr{B}_6}}{2\mathscr{B}_4}\end{aligned} \tag{37}$$

where $\mathscr{B}_1 = \mathscr{D}_\epsilon$, $\mathscr{B}_2 = \|\tilde{\tau}_{hum}\|$, $\mathscr{B}_3 = \mathscr{D}_{\tau_2}\,\|\tilde{\tau}_{hum}\|$, $\mathscr{B}_4 = \mathscr{D}_{\tau_1}$, $\mathscr{B}_5 = \|\epsilon_q\| + \mathscr{D}_{\tau_2}$ and $\mathscr{B}_6 = \mathscr{D}_\epsilon$.

According to the above analysis, the positive definite Lyapunov function declines outside of the bounded region introduced in Eq. (37). Therefore, the convergence to this compact region is achieved whose dimensions are obtained regarding the bounded time derivative of the HRI torque ($\dot{\tau}_{hum}$). This guarantees the UUB of the system response in terms of the bounded trajectory tracking error ϵ_q (and consequently e_q) and the bounded HRI torque estimation error $\tilde{\tau}_{hum}$ in (37). Thereby, the closed-loop exoskeleton system interacting with the human user is stable under the assumption of bounded-varying interaction torque ($||\dot{\tau}_{hum}|| \leq \rho_{\tau_d}$) employing the proposed TBA disturbance-observer-based nonlinear strategy for the low-level control. ■

IV. Experimental Studies

In order to evaluate the performance of the developed autonomous control scheme and assess its adaptive features in high and low levels, comprehensive experiments were conducted on the Indego exoskeleton (Parker Hannifin Corporation) as the testbed. Two able-bodied wearers (33 and 27 years of age) wore the exoskeleton as shown in Fig. 3 and performed the locomotion experiment with a minimum duration of 100 sec. To implement the proposed controller, the major computational effort consists of the time integration

(a) (b)

Fig. 3. Indego lower-limb exoskeleton worn by two able-bodied users for overground walking: (a) first participant (33 year-old) and (b) second participant (27 year-old)

	Hip initial motion	Knee initial motion
Coefficients of Fourier series	$a_0 = 10.13$ $a_1 = 21.80,\ a_2 = -5.07$ $a_3 = -0.49,\ a_4 = -0.52$ $a_5 = 0.20,\ a_6 = -0.07$ $a_7 = -0.09,\ a_8 = -0.09$ $b_1 = -10.77,\ b_2 = -2.21$ $b_3 = 1.86,\ b_4 = 0.41$ $b_5 = 0.20,\ b_6 = -0.06$ $b_7 = -0.05,\ b_8 = -0.05$	$a_0 = 22.44$ $a_1 = -2.93,\ a_2 = -14.32$ $a_3 = 0.05,\ a_4 = -0.38$ $a_5 = 0.36,\ a_6 = 0.20$ $a_7 = -0.01,\ a_8 = 0.03$ $b_1 = -26,48,\ b_2 = 9.81$ $b_3 = 4.44,\ b_4 = 1.87$ $b_5 = 0.59,\ b_6 = -0.15$ $b_7 = -0.08,\ b_8 = -0.07$

TABLE I
COEFFICIENTS OF THE FOURIER SERIES (7) FOR THE HIP AND KNEE INITIAL MOTIONS BASED ON THE ANALYSIS OF NORMAL GAIT TRAJECTORIES

	Hip and knee CPGs' parameters
Dynamic parameter values	$\gamma_{h-h} = 0.0075,\ \gamma_{h-k} = 0.0075,$ $\gamma_{k-h} = 0.0075,\ \beta_\omega = 10\pi,\ \beta_\mu = 10\pi,$ $\psi = 0.0045\ \lambda = 0.006,\ \Omega = \frac{\pi}{2},\ A = 1$
Initial values	$\theta_{right}(0) = 2\ rad,\ \theta_{left}(0) = 2 + \pi\ rad,\ \omega(0) = 1.26\ rad/s,\ \mu(0) = 1$

TABLE II
PARAMETER AND INITIAL VALUES OF THE PROPOSED ACPGS DYNAMICS (6) FOR THE HIP AND KNEE JOINTS

of the CPG dynamics (6) and Eqs. (17), (25), (31) in the disturbance observer structure, as well as performing the required calculations to command the control law (9) for each joint of the exoskeleton. The proposed strategy was implemented in the real-time MATLAB-Simulink environment running on a PC (Intel Core i7-8650U CPU @ 1.90GHz and 8.00 GB RAM) and required communications (between sensors, PC, and actuators), and the required computations were conducted with the sampling time of 5 msec. Preliminary tests were first conducted to identify the passive dynamic parameters of the combined exoskeleton-human limb system to implement the proposed torque control law accurately.

The initial hip and knee trajectories were extracted from motion capture data of typical human locomotion in the literature [44], [45]. To acquire this experimental data, the subject walked for at least 20 sec in each trial for a total of approximately 1 hour and 10 min (with more than 3600 gait cycles). A marker-based motion capture system was employed to obtain 2D joint angles and velocities. A Fourier analysis was conducted on the acquired trajectories to obtain the minimum adequate number of series and identify the best values of corresponding coefficients. Eight terms of the Fourier series ($N_i = 8$ in (7)) were sufficient to estimate these hip and knee motions with the sine and cosine functions. Attained coefficients of the Fourier series for the hip and knee motions based on this analysis are listed in Table I, which resulted in estimation of the typical gait [44], [45] with more than 98% accuracy for each joint.

Parameters and initial values of the proposed ACPG dynamics for the hip and knee joints of both legs are listed in Table II. The initial phase difference of π rad was considered between the left and right legs' motions, as is the case for typical bipedal locomotion. The estimated HRI torques of all joints, determined based on the TBA observer law (31) and the defined dead-zone function (5), are shown in Fig. 4(a) for the first wearer (33 year-old participant). The corresponding HRI energy transferred through each joint and obtained by (4) and the total value of this energy are demonstrated in Fig. 4(b) for this experiment. As seen, this wearer applied the major torques over the first four steps (with a maximum magnitude of 7.1 N.m) to personalize the gait motion. According to Figs. 4(a) and 4(b), he injected most of the HRI energy by the right hip torque and then the right knee torque to accelerate the motion, while he applied decelerating torques on the left knee joint to control the gait. The effect of this interaction on the variation of the total locomotion frequency $\omega(t)$ is depicted in Fig. 4(c). Rapid online response of the ACPG (6) to these interactions was achieved during each stride. The steady-state magnitude of the locomotion frequency in Fig. 4(c) had a 42% increase with respect to its initial magnitude of 1.17 rad/s and finally settled on 1.66$\pm$0.02 rad/s.

Due to this real-time update of ACPG and the obtained Fourier coefficients in Table I, the desired locomotion trajectories, generated by (7) for the right knee and hip joints, are shown in Fig. 5(a) together with the exoskeleton response. The first human user applied the interaction torques in sequential steps (Fig. 4(a)) to modify and increase the gait amplitude (step size) by 15% (Fig. 5(a)) in addition to the walking frequency (Fig. 4(c)), which provided a synchronized variation of the generated bipedal locomotion cycles. The proposed TBA disturbance-observer-based torque controller could facilitate an appropriate convergence of joint positions to the desired gait trajectories with a small bounded tracking error e_q in the steady-state response (less than 1 degree for each joint), as presented in Fig. 5(b). This is in accordance with the stability analysis in Sec. III-B and implies an appropriate estimation of the HRI torque with a small bounded error $\tilde{\tau}_{hum}$, employing the disturbance observer defined in Sec. III-A.

In order to elaborate more on the autonomous shaping of locomotion, the reference trajectory and phase variation of the right hip with respect to the left hip are plotted in Fig. 6 for the first wearer. The increase of 15% in total gait amplitude

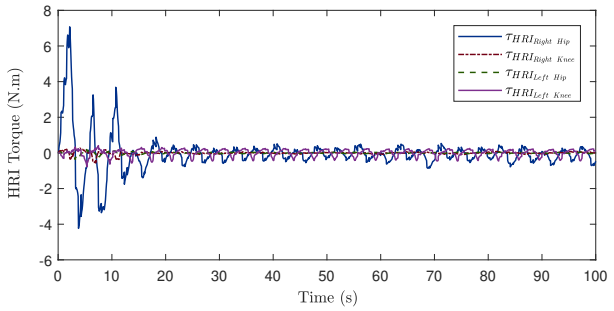

(a)

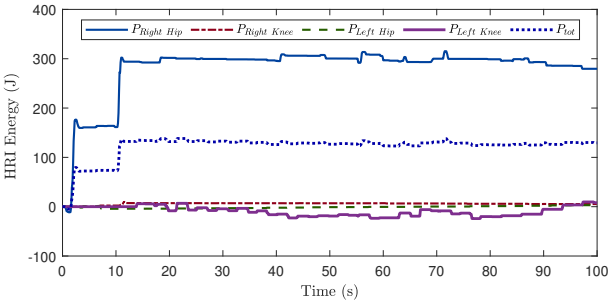

(b)

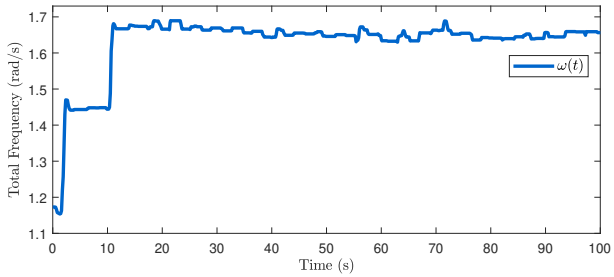

(c)

Fig. 4. Estimated HRI (a) torque and (b) energy for different joints, and (c) total frequency of the locomotion, obtained from the proposed ACPG in the presence of HRI for the first wearer

$\mu(t)$ and its convergence to a steady-state response, together with the relative motion adjustments of adjacent joints, are illustrated in these diagrams. Accordingly, the desired ranges of motion of the knee and hip joints were amended to 78.7 and 61.2 degrees, respectively, from 68.4 and 53.2 degrees. As shown in Fig. 6, an average phase lead of 13.0 degrees in the right hip motion was eventually obtained over the left hip motion in addition to their initial phase difference of 180 degrees, due to the asymmetric rendering of the interaction torques (Fig. 4(b)).

For the second wearer (27 year-old participant), the estimation of HRI torques and corresponding HRI energy (4) transferred through different joints are represented in Figs. 7(a) and 7(b). This wearer exerted the major torques over the first six steps (with a maximum magnitude of 3.61 N.m) to adjust his locomotion pattern. As observed in Figs. 7(a) and 7(b), this wearer transferred most of the energy through the left hip and then the right hip to accelerate the gait. The variation of the locomotion frequency $\omega(t)$ in response to this HRI is shown in Fig. 7(c) with a steady-state variation of 53% compared to its initial magnitude of 1.17 rad/s. The generated reference trajectory and phase variation of the right hip with respect to the left hip is illustrated for the second participant in Fig. 8.

V. Discussion

Due to the adaptiveness of the proposed CPG-based control strategy, the obtained locomotion trajectories were personalized for the two participants engaged in this study. As seen in Fig. 4, the first wearer (33 year-old participant) injected 73% of accelerating energy by the right hip torque and 24% by the right knee torque. However, the second wearer (27 year-old participant) modified his gait frequency by transferring 69% and 29% of positive HRI energy via the left hip and right hip joints, respectively, to accelerate the locomotion, as demonstrated in Fig. 7. This implies a significant difference in HRI over hip joints of the lower-limb exoskeleton between the first and second wearers, in regard to the modification of the locomotion pattern. In addition to this HRI difference in various joints, the second wearer came up with a final locomotion frequency with 11% more increase from its initial value in comparison with the one achieved by the first wearer. Furthermore, the second wearer made this gait adjustment in 23 sec (over 6 steps), which was 35% longer than the time duration of 15 sec spent by the first wearer to modify his walking pattern (over 4 steps).

An analysis of the relative joint trajectories and phase variations in Figs. 6 and 8 can provide additional insight into this personalized gait amendment. The second participant decided to raise his steady-state gait amplitude $\mu(t)$ by 13% (Fig. 8) which is slightly less than the 15% increment provided by the first participant (Fig. 6). This difference was due to the larger height (longer body segments of the lower limbs) of the first participant and their personal preferences for the step size in their natural walking. The other significant differences between two wearers' performance achieved by employing the proposed intelligent control strategy were the synchronization and phase shifts between the hip and knee joints. Figure 8 shows that the second participant made an average phase lag of 4.8 degrees in the right hip motion relative to the left hip; however, the first participant made an average phase lead of 13.1 degrees between these joints' motions (Fig. 8). As a result of this difference, the distortion of the relative trajectories in Fig. 6 for the first wearer was more toward the bottom right as compared to the variation in Fig. 8 for the second wearer, which was more toward the top left. This is due to rendering most (73%) of the accelerating interaction torques on the right hip by the first wearer (Fig. 4(b)) rather than the left hip that was employed for applying 69% of the accelerating torques by the second wearer (Fig. 7(b)). This performance implies adjustable flexibility in locomotion speed and amplitude, and modification of the synchronization between different joints using the proposed adaptive CPG-based control strategy for the lower-limb exoskeleton in response to the estimated interaction torques.

VI. Conclusion

A new autonomous control scheme was developed in this work to facilitate flexible and personalized locomotion based on HRI for lower-limb exoskeletons. At the higher level of this scheme, ACPGs were proposed to update the frequency

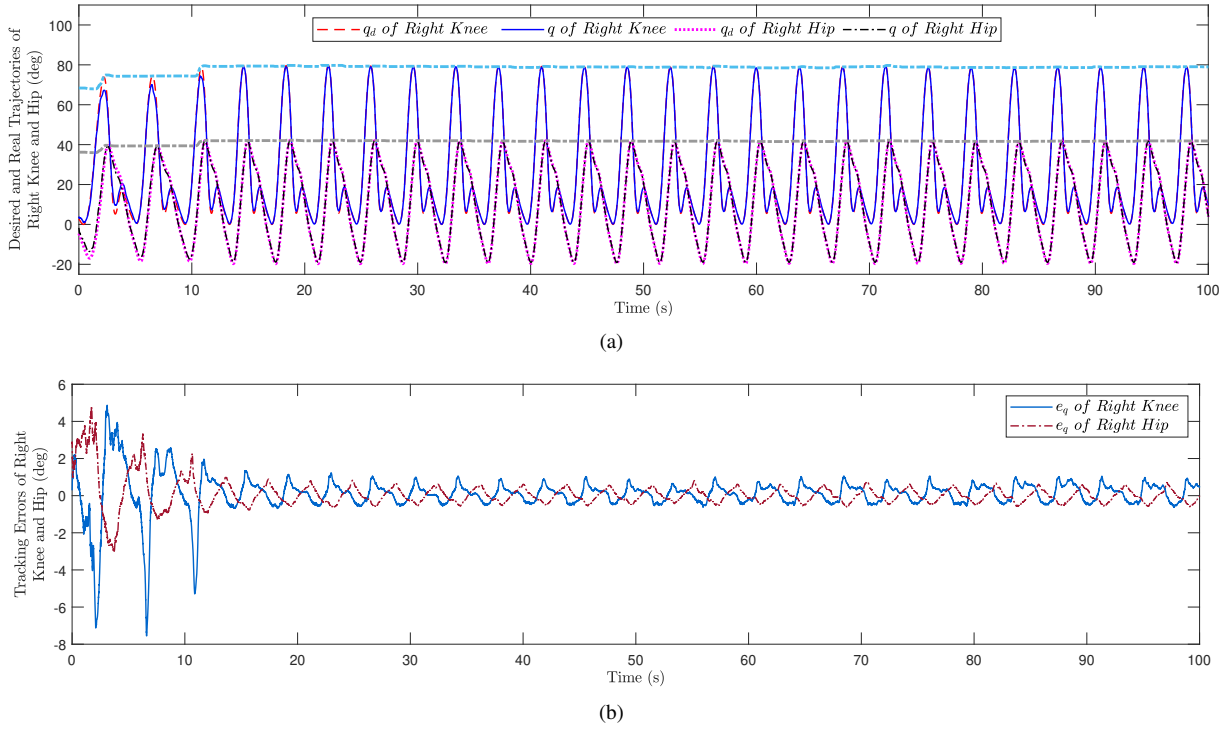

Fig. 5. (a) Desired and actual trajectories, (b) and (c) tracking errors of the knee and hip joints for the right leg in the presence of HRI for the first wearer

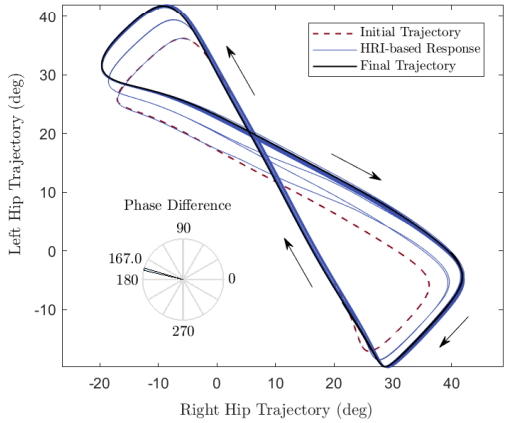

Fig. 6. Trajectory and phase variation of the right hip with respect to the left hip for the first wearer

and amplitude of desired gait trajectories for all exoskeleton joints. Simultaneously, the ACPGs were responsible for synchronizing adjacent joints' motions by adjusting their phase differences. These adaptations were defined based on the estimation of HRI torque and its corresponding energy.

For the low-level control, a multi-layer TBA disturbance observer integrated into a nonlinear torque controller was investigated to estimate and compensate for the HRI interaction torque and to track the desired locomotion trajectories. In addition, this torque estimation was also employed in high-level CPG-based motion planning. The exoskeleton's closed-loop stability was ensured via a Lyapunov analysis such that the UUB of the trajectory tracking error and the torque estimation error was guaranteed.

The developed autonomous control strategy was evaluated experimentally using the Indego exoskeleton (Parker Hannifin Corporation) and having an able-bodied wearer. Smooth and rapid shaping of the gait trajectories was achieved using the proposed ACPGs in real-time for various arbitrary interactions over different joints. Wearers amended the locomotion frequency and amplitude by up to 53% and 15%, respectively, and modified the phase synchronization between hip motions by up to 13% due to their individual preferences. Appropriate tracking performance of the nonlinear torque controller with a small bounded error (less than 1 degree for each joint) was obtained due to the precise estimation of the interaction torque via the proposed TBA disturbance observer.

ACKNOWLEDGMENT

The authors would like to thank Dr. Vahid Azimi at Auburn University for the his constructive comments on the observer design and provided locomotion data.

This work was supported by the Natural Sciences and Engineering Research Council, Canadian Institutes of Health Research, Canada Foundation for Innovation, the Government of Alberta (Department of Economic Development, Trade and Tourism) and Parker Hannifin Corporation. VKM is a Canada Research Chair (Tier 1) in Functional Restoration. MS is a recipient of a postdoctoral fellowship award from the SMART Network Innovation Fund.

REFERENCES

[1] H. S. Park, Y. Ren, and L. Q. Zhang, "Intelliarm: An exoskeleton for diagnosis and treatment of patients with neurological impairments," in *IEEE RAS & EMBS International Conference on Biomedical Robotics and Biomechatronics*, 2008, pp. 109–114.

[2] H. S. Lo and S. Q. Xie, "Exoskeleton robots for upper-limb rehabilitation: State of the art and future prospects," *Medical Engineering & Physics*, vol. 34, no. 3, pp. 261–268, 2012.

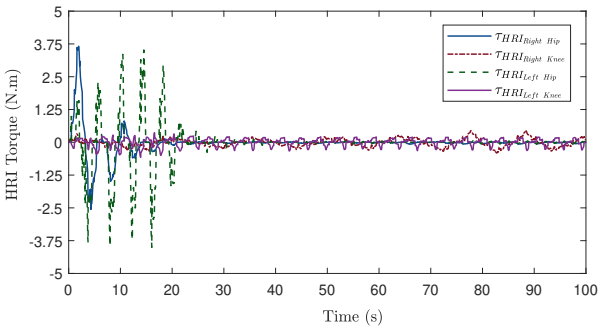

(a)

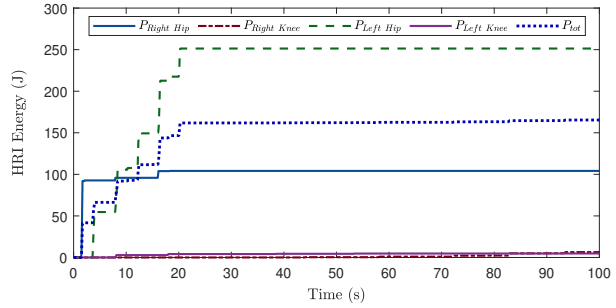

(b)

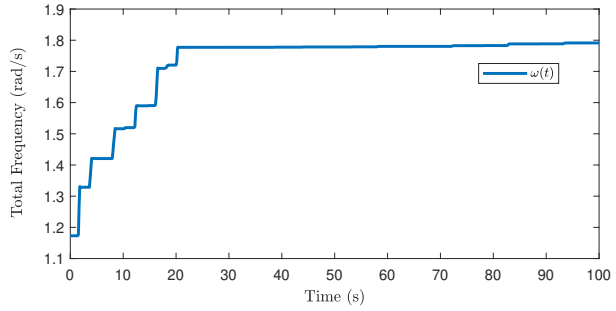

(c)

Fig. 7. Estimated HRI (a) torque and (b) energy for different joints, and (c) total frequency of the locomotion, obtained from the proposed ACPG in the presence of HRI for the second wearer

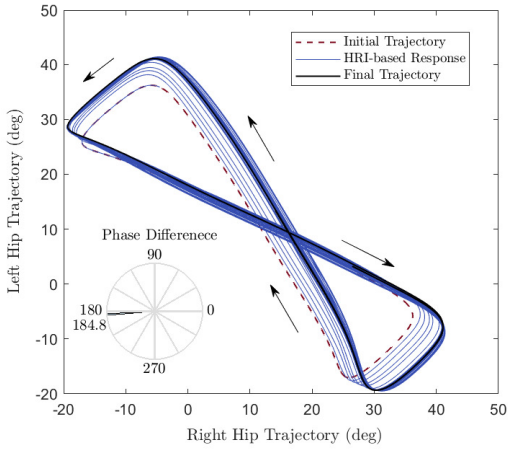

Fig. 8. Trajectory and phase variation of the right hip with respect to the left hip for the second wearer

[3] S. A. Murray, R. J. Farris, M. Golfarb, C. Hartigan, C. Kandilakis, and D. Truex, "Fes coupled with a powered exoskeleton for cooperative muscle contribution in persons with paraplegia," in *Annual International Conference of the IEEE Engineering in Medicine and Biology Society (EMBC)*, 2018, pp. 2788–2792.

[4] G. Zeilig, H. Weingarden, M. Zwecker, I. Dudkiewicz, A. Bloch, and A. Esquenazi, "Safety and tolerance of the rewalk™ exoskeleton suit for ambulation by people with complete spinal cord injury: a pilot study," *The Journal of Spinal Cord Medicine*, vol. 35, no. 2, pp. 96–101, 2012.

[5] Y. Lee, J. Lee, B. Choi, M. Lee, S.-g. Roh, K. Kim, K. Seo, Y.-J. Kim, and Y. Shim, "Flexible gait enhancing mechatronics system for lower limb assistance (gems l-type)," *IEEE/ASME Transactions on Mechatronics*, vol. 24, no. 4, pp. 1520–1531, 2019.

[6] A. Esquenazi, M. Talaty, and A. Jayaraman, "Powered exoskeletons for walking assistance in persons with central nervous system injuries: a narrative review," *PM&R*, vol. 9, no. 1, pp. 46–62, 2017.

[7] Z. Li, K. Zhao, L. Zhang, X. Wu, T. Zhang, Q. Li, X. Li, and C.-Y. Su, "Human-in-the-loop control of a wearable lower limb exoskeleton for stable dynamic walking," *IEEE/ASME Transactions on Mechatronics*, pp. 1–1, 2020.

[8] C. Buesing, G. Fisch, M. O'Donnell, I. Shahidi, L. Thomas, C. K. Mummidisetty, K. J. Williams, H. Takahashi, W. Z. Rymer, and A. Jayaraman, "Effects of a wearable exoskeleton stride management assist system (sma®) on spatiotemporal gait characteristics in individuals after stroke: a randomized controlled trial," *Journal of neuroengineering and rehabilitation*, vol. 12, no. 1, pp. 1–14, 2015.

[9] Y. Lee, S.-g. Roh, M. Lee, B. Choi, J. Lee, J. Kim, H. Choi, Y. Shim, and Y.-J. Kim, "A flexible exoskeleton for hip assistance," in *2017 IEEE/RSJ International Conference on Intelligent Robots and Systems (IROS)*. IEEE, 2017, pp. 1058–1063.

[10] C. A. McGibbon, A. Sexton, A. Jayaraman, S. Deems-Dluhy, P. Gryfe, A. Novak, T. Dutta, E. Fabara, C. Adans-Dester, and P. Bonato, "Evaluation of the keeogo exoskeleton for assisting ambulatory activities in people with multiple sclerosis: an open-label, randomized, cross-over trial," *Journal of neuroengineering and rehabilitation*, vol. 15, no. 1, pp. 1–14, 2018.

[11] K. Gui, H. Liu, and D. Zhang, "A practical and adaptive method to achieve emg-based torque estimation for a robotic exoskeleton," *IEEE/ASME Transactions on Mechatronics*, vol. 24, no. 2, pp. 483–494, 2019.

[12] S. Kim and J. Bae, "Force-mode control of rotary series elastic actuators in a lower extremity exoskeleton using model-inverse time delay control," *IEEE/ASME Transactions on Mechatronics*, vol. 22, no. 3, pp. 1392–1400, 2017.

[13] Y. Yang, X. Dong, X. Liu, and D. Huang, "Robust repetitive learning-based trajectory tracking control for a leg exoskeleton driven by hybrid hydraulic system," *IEEE Access*, vol. 8, pp. 27 705–27 714, 2020.

[14] S. Schaal, "Dynamic movement primitives-a framework for motor control in humans and humanoid robotics," in *Adaptive motion of animals and machines*. Springer, 2006, pp. 261–280.

[15] Y. Yuan, Z. Li, T. Zhao, and D. Gan, "Dmp-based motion generation for a walking exoskeleton robot using reinforcement learning," *IEEE Transactions on Industrial Electronics*, 2019.

[16] S. Qiu, W. Guo, D. Caldwell, and F. Chen, "Exoskeleton online learning and estimation of human walking intention based on dynamical movement primitives," *IEEE Transactions on Cognitive and Developmental Systems*, 2020.

[17] R. Huang, H. Cheng, J. Qiu, and J. Zhang, "Learning physical human–robot interaction with coupled cooperative primitives for a lower exoskeleton," *IEEE Transactions on Automation Science and Engineering*, vol. 16, no. 4, pp. 1566–1574, 2019.

[18] A. Sproewitz, R. Moeckel, J. Maye, and A. J. Ijspeert, "Learning to move in modular robots using central pattern generators and online optimization," *The International Journal of Robotics Research*, vol. 27, no. 3-4, pp. 423–443, 2008.

[19] M. Sharifi, J. K. Mehr, V. K. Mushahwar, and M. Tavakoli, "Adaptive cpg-based gait planning with learning-based torque estimation and control for exoskeletons," *IEEE Robotics and Automation Letters*, vol. 6, no. 4, pp. 8261–8268, 2021.

[20] A. J. Ijspeert, A. Crespi, D. Ryczko, and J.-M. Cabelguen, "From swimming to walking with a salamander robot driven by a spinal cord model," *science*, vol. 315, no. 5817, pp. 1416–1420, 2007.

[21] W. Wang, L. Qin, X. Yuan, X. Ming, T. Sun, and Y. Liu, "Bionic control of exoskeleton robot based on motion intention for rehabilitation training," *Advanced Robotics*, vol. 33, no. 12, pp. 590–601, 2019.

[22] J. Fang, Y. Ren, and D. Zhang, "A robotic exoskeleton for lower limb rehabilitation controlled by central pattern generator," in *2014 IEEE*

International Conference on Robotics and Biomimetics (ROBIO 2014). IEEE, 2014, pp. 814–818.
[23] S. O. Schrade, Y. Nager, A. R. Wu, R. Gassert, and A. Ijspeert, "Bio-inspired control of joint torque and knee stiffness in a robotic lower limb exoskeleton using a central pattern generator," in *International Conference on Rehabilitation Robotics (ICORR)*, 2017, pp. 1387–1394.
[24] R. Luo, S. Sun, X. Zhao, Y. Zhang, and Y. Tang, "Adaptive cpg-based impedance control for assistive lower limb exoskeleton," in *2018 IEEE International Conference on Robotics and Biomimetics (ROBIO)*. IEEE, 2018, pp. 685–690.
[25] K. Gui, H. Liu, and D. Zhang, "A generalized framework to achieve coordinated admittance control for multi-joint lower limb robotic exoskeleton," in *International Conference on Rehabilitation Robotics (ICORR)*, 2017, pp. 228–233.
[26] D. Zhang, Y. Ren, K. Gui, J. Jia, and W. Xu, "Cooperative control for a hybrid rehabilitation system combining functional electrical stimulation and robotic exoskeleton," *Frontiers in Neuroscience*, vol. 11, p. 725, 2017.
[27] M. Sharifi et al., "Impedance variation and learning strategies in human-robot interaction," *IEEE Transactions on Cybernetics*, pp. 1–14, 2021.
[28] ——, "Impedance learning-based adaptive control for human-robot interaction," *IEEE Transactions on Control Systems Technology*, pp. 1–14, 2021.
[29] Q. Wei, Z. Li, K. Zhao, Y. Kang, and C.-Y. Su, "Synergy-based control of assistive lower-limb exoskeletons by skill transfer," *IEEE/ASME Transactions on Mechatronics*, vol. 25, no. 2, pp. 705–715, 2020.
[30] T. Zhang, M. Tran, and H. Huang, "Design and experimental verification of hip exoskeleton with balance capacities for walking assistance," *IEEE/ASME Transactions on Mechatronics*, vol. 23, no. 1, pp. 274–285, 2018.
[31] X. Liu and Q. Wang, "Real-time locomotion mode recognition and assistive torque control for unilateral knee exoskeleton on different terrains," *IEEE/ASME Transactions on Mechatronics*, vol. 25, no. 6, pp. 2722–2732, 2020.
[32] C. F. Chen, Z. J. Du, L. He, Y. J. Shi, J. Q. Wang, G. Q. Xu, Y. Zhang, D. M. Wu, and W. Dong, "Development and hybrid control of an electrically actuated lower limb exoskeleton for motion assistance," *IEEE Access*, vol. 7, pp. 169 107–169 122, 2019.
[33] L. Liu, S. Leonhardt, C. Ngo, and B. J. Misgeld, "Impedance-controlled variable stiffness actuator for lower limb robot applications," *IEEE Transactions on Automation Science and Engineering*, 2019.
[34] C. T. Pan, C. C. Chang, Y. S. Yang, C. K. Yen, C. C. Liu, C. L. Lee, and Y. L. Shiue, "Development a multi-loop modulation method on the servo drives for lower limb rehabilitation exoskeleton," *Mechatronics*, vol. 68, p. 102360, 2020.
[35] W. Huo, M. A. Alouane, Y. Amirat, and S. Mohammed, "Force control of sea-based exoskeletons for multimode human–robot interactions," *IEEE Transactions on Robotics*, 2019.
[36] W. Huo, S. Mohammed, and Y. Amirat, "Impedance reduction control of a knee joint human-exoskeleton system," *IEEE Transactions on Control Systems Technology*, vol. 27, no. 6, pp. 2541–2556, 2018.
[37] F. Ghorbel, B. Srinivasan, and M. W. Spong, "On the uniform boundedness of the inertia matrix of serial robot manipulators," *Journal of Robotic Systems*, vol. 15, no. 1, pp. 17–28, 1998.
[38] J. Slotine and W. Li, *Applied Nonlinear Control*. Prentice-Hall, 1991.
[39] M. Sharifi, "Impedance control of non-linear multi-dof teleoperation systems with time delay: absolute stability," *IET Control Theory & Applications*, vol. 12, pp. 1722–1729(7), 2018.
[40] A. J. Ijspeert, A. Crespi, D. Ryczko, and J.-M. Cabelguen, "From swimming to walking with a salamander robot driven by a spinal cord model," *Science*, vol. 315, no. 5817, pp. 1416–1420, 2007.
[41] P. Ioannou and J. Sun, *Robust Adaptive Control*, ser. Dover Books on Electrical Engineering Series. Dover Publications, Incorporated, 2012.
[42] M. N. Mahyuddin, J. Na, G. Herrmann, X. Ren, and P. Barber, "Adaptive observer-based parameter estimation with application to road gradient and vehicle mass estimation," *IEEE Transactions on Industrial Electronics*, vol. 61, no. 6, pp. 2851–2863, 2014.
[43] S. Sastry and M. Bodson, *Adaptive Control: Stability, Convergence and Robustness*. Dover Publications, 2011.
[44] V. Azimi, D. Simon, and H. Richter. Kinematic and kinetic human gait data for able-bodied and transfemoral amputee subjects. [Online]. Available: https://www.vahidazimi.com/data-code
[45] V. Azimi, S. Abolfazl Fakoorian, T. Tien Nguyen, and D. Simon, "Robust adaptive impedance control with application to a transfemoral prosthesis and test robot," *Journal of Dynamic Systems, Measurement, and Control*, vol. 140, no. 12, 2018.

Mojtaba Sharifi is an Assistant Professor at the Department of Mechanical Engineering, San Jose State University, San Jose, California, USA. Prior to that, he was a postdoctoral research fellow at the Department of Electrical and Computer Engineering and the Department of Medicine, University of Alberta, Canada. He received his B.Sc. and M.Sc. degrees in Mechanical Engineering from Shiraz University and Sharif University of Technology, Iran, in 2010 and 2012, respectively. He conducted a collaborative research project in the Telerobotic and Biorobotic Systems Lab of the University of Alberta, Canada, from 2015 to 2016, and earned his Ph.D. degree from Sharif University of Technology, Iran, in 2017. His interdisciplinary research includes intelligent control, dynamics and design of robots (in biomedical applications: rehabilitation, surgery and imaging), human-robot interaction (using impedance control and learning), haptics, collaborative robotics and tele-robotics (using bilateral and multilateral control), wearable and assistive robotics (exoskeleton, prosthesis and orthosis), control and modeling of musculoskeletal systems, and biological systems.

Javad K. Mehr received his B.Sc. and M.Sc. degrees in Mechanical Engineering from the University of Tabriz in 2015 and Shiraz University in 2019. He is currently pursuing a Ph.D. degree in the Department of Electrical and Computer Engineering and the Department of Medicine at the University of Alberta. His research interests are modeling and controlling robotic systems in medical applications with a focus on lower-limb rehabilitation.

Vivian K. Mushahwar received her B.Sc. degree in electrical engineering from Brigham Young University, Provo, UT, USA in 1991 and a Ph.D. degree in bioengineering from the University of Utah, Salt Lake City, USA in 1996. She received postdoctoral training at Emory University, Atlanta, GA, USA and the University of Alberta, Edmonton, AB, Canada. She is currently a professor in the Department of Medicine, Division of Physical Medicine and Rehabilitation at the University of Alberta, a Canada Research Chair (Tier 1) in Functional Restoration, and a Killam Professor. She is also the director of the Sensory Motor Adaptive Rehabilitation Technology (SMART) Network at the University of Alberta. Her research interests include identification of spinal-cord systems involved in locomotion, development of spinal-cord-based neural prostheses for restoring mobility after spinal cord injury, identification of rehabilitation interventions for enhancing mobility, and the use of active intelligent wearable devices for preventing secondary complications associated with neurological conditions including spasticity, pressure injuries, and deep vein thrombosis.

Mahdi Tavakoli is a Professor in the Department of Electrical and Computer Engineering, University of Alberta, Canada. He received his BSc and MSc degrees in Electrical Engineering from Ferdowsi University and K.N. Toosi University, Iran, in 1996 and 1999, respectively. He received his PhD degree in Electrical and Computer Engineering from the University of Western Ontario, Canada, in 2005. In 2006, he was a post-doctoral researcher at Canadian Surgical Technologies and Advanced Robotics (CSTAR), Canada. In 2007-2008, he was an NSERC Post-Doctoral Fellow at Harvard University, USA. Dr. Tavakoli's research interests broadly involve the areas of robotics and systems control. Specifically, his research focuses on haptics and teleoperation control, medical robotics, and image-guided surgery. Dr. Tavakoli is the lead author of Haptics for Teleoperated Surgical Robotic Systems (World Scientific, 2008). He is a Senior Member of IEEE and an Associate Editor for IEEE/ASME Transactions on Mechatronics, Journal of Medical Robotics Research, Control Engineering Practice, and Mechatronics.